



## Piezo-promoted the generation of reactive oxygen species and the photodegradation of organic pollutants

Yao Chen, Xiaoming Deng, Jieya Wen, Jian Zhu, Zhenfeng Bian\*

The Education Ministry Key Laboratory of Resource Chemistry and Shanghai Key Laboratory of Rare Earth Functional Materials, Shanghai Normal University, Shanghai, 200234, PR China



### ARTICLE INFO

**Keywords:**  
Piezoelectric effect  
Photocatalysis  
FeTCPP/MoS<sub>2</sub>  
Synergistic effect

### ABSTRACT

Composite of porphyrins and piezoelectric materials is a promising method to overcome the limitation of photocatalytic response of composite catalysts, inhibit photogenerated electron-hole recombination and enhance photocatalytic degradation performance. Here, the Fe-S electronic channel is formed by the combination of MoS<sub>2</sub> and iron porphyrin, which enhances the electron transfer performance of iron porphyrin to MoS<sub>2</sub> semiconductor. At the same time, two-dimensional MoS<sub>2</sub> surface with piezoelectric properties forms an electric field, which further enhances charge separation and piezoelectric catalytic performance. The photoexcitation of porphyrin and the piezoelectric excitation of molybdenum sulfide cooperate with each other under the simultaneous action of light and ultrasound. Oxygen radicals and hydroxyl radicals are enhanced, and the catalytic degradation performance is further enhanced. By strengthening the interaction between porphyrins and piezoelectric materials, especially bonding, a good and stable catalyst for pollutant degradation and purification was prepared.

### 1. Introduction

At present, advanced oxidation methods (AOPs) for degradation of organic pollutants include photochemical oxidation, catalytic wet oxidation, sonochemical oxidation, ozone oxidation, electrochemical oxidation, Fenton oxidation, etc [1–6]. Photocatalytic technology is a potential advanced oxidation technology developed in recent years because of its mild reaction conditions and direct use of sunlight [7–10]. However, the rapid recombination of photogenerated electrons and holes is the main limitation of photocatalytic technology [11,12]. There are several ways to inhibit the photogenerated electron-hole recombination process to enhance activity, such as introducing defects [13–19], dyes sensitization [20–22], noble metals [23–27] and carbon material modification [28–30], heterojunctions [31–39], etc.

It is well-known that biomimetic photocatalytic degradation of organic pollutants has attracted wide attention, especially the photocatalyst based on metalloporphyrins [40]. Porphyrin molecules form highly ordered aggregation structure, which can effectively absorb visible light [41]. As an antenna molecule, long-range charge transport between molecules eventually injects charge into the catalytic reaction center to complete effective photosynthesis. In general, iron porphyrin is considered as a promising biomimetic photocatalyst [42]. However, there are inherent defects in the direct use of iron porphyrin as a photocatalyst for oxidation reaction: iron porphyrin molecules are easy

to condense into dimers, while dimers have no photocatalytic activity and are easy to oxidize and decompose in the photocatalytic system [43]. Therefore, the photocatalytic activity and stability of porphyrins can be effectively improved by the combination of inorganic semiconductor materials and porphyrins, as well as the optical absorption and charge separation of porphyrins [20].

In recent years, MoS<sub>2</sub> has attracted extensive attention due to its unique properties in electronics, optics, photocatalysis and piezoelectricity [44–47]. Heterojunction structures are formed by composite semiconductor materials such as MoS<sub>2</sub>/TiO<sub>2</sub> and MoS<sub>2</sub>/BiVO<sub>4</sub>, which exhibit enhanced photocatalytic properties in the ultraviolet and visible regions [48,49]. Jyh Ming Wu et al. have shown that single or few layers of molybdenum sulfide have piezoelectric catalytic properties [50]. When applied by external force, due to its spontaneous polarization, an electric field is formed inside molybdenum sulfide, which can effectively separate free carriers of electrons and holes, and realize the catalytic decomposition of organic pollutants by molybdenum sulfide under no light conditions. The combination of photocatalyst and piezoelectric catalysis, the use of built-in electric field of piezoelectric materials to separate photogenerated charges in space and improve the photocatalytic activity of photocatalyst is also important directions of photocatalytic research [51–58]. However, the study of composite photocatalysts on molybdenum sulfide piezoelectric materials is very limited.

\* Corresponding author.

E-mail address: [bianzhenfeng@shnu.edu.cn](mailto:bianzhenfeng@shnu.edu.cn) (Z. Bian).

Herein, we reported ferroporphyrin with photocatalytic activity and layered molybdenum sulfide with piezoelectric properties are combined to achieve enhanced catalytic degradation performance. In iron porphyrins, photo stimulated porphyrin ligands produce photogenerated electrons that are transferred to metal centers and to  $\text{MoS}_2$  via electronic channels, thus separating electron holes. The surface of molybdenum sulfide forms piezoelectric field under the action of ultrasonic wave, which rapidly separates free carriers improving the catalytic performance. The composite material is stable and has good degradation performance for various organic pollutants.

## 2. Experimental section

### 2.1. Catalyst preparation

All chemicals used in this study were analytical grade (Sigma Aldrich) without further purification.  $\text{MoS}_2$  with piezoelectric effect was synthesized by the reported method [50]. FeTCPP monomer was prepared by a reflux reaction. In a typical synthesis, 60 mg porphyrin (TCPP) and 100 mg  $\text{FeCl}_3$  were added in 150 ml DMF. The mixed reaction solution was transferred to a round bottom flask. After stirring, the solvent DMF was heated to 150 °C, cooled and distilled under vacuum. After being dispersed in ethanol, the filtrate is concentrated and dried to obtain green solid powder (FeTCPP).

The FeTCPP (as-prepared) was dissolved in 100 ml absolute ethanol and 2.0 g  $\text{MoS}_2$  was added. Mixture was transferred to autoclave and reacted at 170 °C for 10 h. FeTCPP/ $\text{MoS}_2$  was synthesized by centrifugation and ethanol washing. The samples were denoted as x% FeTCPP/ $\text{MoS}_2$ , where x% represent the mass percentage of FeTCPP and  $\text{MoS}_2$  (Scheme 1). In order to explore the most suitable reaction temperature, we had hydrothermally synthesized 20% FeTCPP/ $\text{MoS}_2$  materials at 150 °C, 160 °C, 180 °C, 190 °C, 200 °C, 210 °C and 220 °C, and tested their catalytic activity by RhB degradation experiments. As the temperature increases, the degradation activity is continuously enhanced, and the material prepared at 170 °C has the best activity. When the temperature continues to rise, the activity of the catalyst gradually decreases (Figs. S1a and S1b).

### 2.2. Characterization

The samples were characterized by field emission scanning electron microscopy (FESEM, HITACHI S4800, operated at 50 kV), transmission electronic micrograph (TEM, JEOL JEM-2010, operated at 200 kV), X-ray photoelectron spectroscopy (XPS, PerkinElmer PHI 5000C, Al  $\text{K}\alpha$ ), Fourier transform infrared spectrometer (FTIR, Nicolet IS 10), UV-vis diffuse reflectance spectra (Shimadzu, UV2600) and X-ray diffraction (XRD, Rigaku D/MAX-2000, Cu  $\text{K}\alpha$  source, operated at 40 kV and 20 mA, scanned at a rate of 5° min<sup>-1</sup>). The Brunauer-Emmett-Teller (BET) method was utilized to calculate the specific surface area. The

electron spin resonance (ESR) spectra of chemical radicals was recorded on a JEOL JES-FA200 model spectrometer to determine the involvement of the reactive oxygen species (ROS). Photoelectrochemical measurements were performed on an electrochemical station (CHI 660E) using a single-compartment quartz cell in a conventional three-electrode system containing a platinum sheet (10mm\*20 mm) counter electrode, a saturated calomel reference electrode (SCE) and the FeTCPP/ $\text{MoS}_2$  film working electrode.

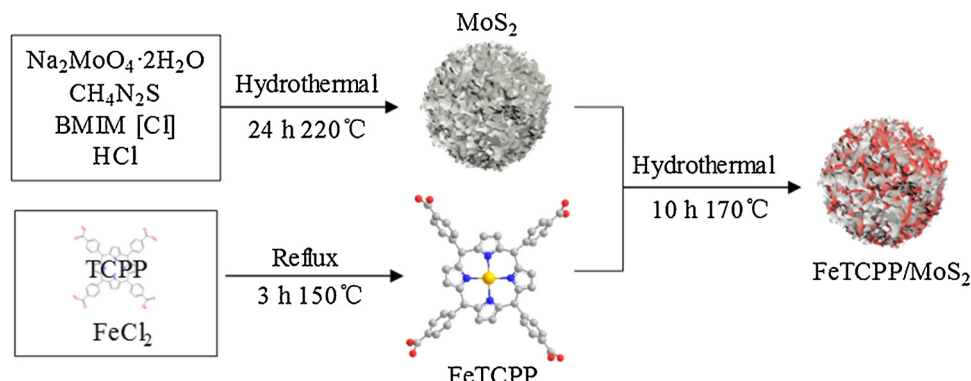
### 2.3. Photocatalytic activity

For typical photocatalytic runs, 50 mg catalyst was dispersed in 50 mL of aqueous solution containing rhodamine B (RhB), methyl orange (MO) or Chlorophenol (4-CP) as probe molecules (10 ppm), which was ultrasonic by an ultrasonic cleaning machine (KX-1613 T, 40KHZ 80 W) and irradiated by a 100 W LED lamp (CEL-LED100, > 420 nm). The solution was stirred for 30 min in the dark before the light and ultrasonic reactions to ensure adsorption equilibrium. The contaminants in the reaction solution are analyzed by a UV spectrophotometer (UV 7502/PC) and Total Organic Carbon (Shimadzu, TOC-VCPN) at the characteristic wavelength, from which the degradation yield was calculated.

## 3. Results and discussions

As shown in Fig. 1a,  $\text{MoS}_2$  sample was nanoflower-like structure with an average diameter around 5  $\mu\text{m}$ . From TEM image (Fig. 1b), it could be seen that the thin sheets of  $\text{MoS}_2$  nanoflower were about three layers thicknesses. The attached Selected-area electron diffraction (SAED) pattern displayed that the  $\text{MoS}_2$  sample had very high crystallinity (inset of Fig. 1b). The morphology of  $\text{MoS}_2$  sample was not affected by the loading of FeTCPP (Fig. 1c). The high resolution TEM (HRTEM) image (Fig. 1d) shows the lamellar structure of the FeTCPP/ $\text{MoS}_2$  sample. Fig. 1e shows the SEM-Mapping image of the FeTCPP/ $\text{MoS}_2$  sample. The FeTCPP on the surface of  $\text{MoS}_2$  was further studied by element distribution. The results of EDX elemental diagram clearly showed that iron elements were uniformly distributed on the surface of  $\text{MoS}_2$ . This proved that FeTCPP was uniformly loaded on the surface of  $\text{MoS}_2$ .

$\text{MoS}_2$  modified by FeTCPP was proved by the characteristic functional group absorption peak of FTIR spectra. The FTIR peaks of 3315 and 965  $\text{cm}^{-1}$  belong to N–H bending vibration peaks for TCPP, while peaks of 1000  $\text{cm}^{-1}$  comes from Fe-N in FeTCPP (Fig. S2) [59]. This shows that iron replaces hydrogen and successfully becomes the metal center of porphyrin. After loading FeTCPP, the peak of FeTCPP/ $\text{MoS}_2$  obviously shows the characteristic peaks of FeTCPP (1760–665  $\text{cm}^{-1}$ ) (Fig. 2a). Based on the calculation from  $\text{N}_2$  adsorption-desorption isotherms, the surface area values ( $S_{\text{BET}}$ ) was slightly decreased with the increase of amount of FeTCPP (Fig. 2b). In comparison with pure  $\text{MoS}_2$ ,



Scheme 1. Schematic illustration for the synthesis of FeTCPP/ $\text{MoS}_2$  sample.

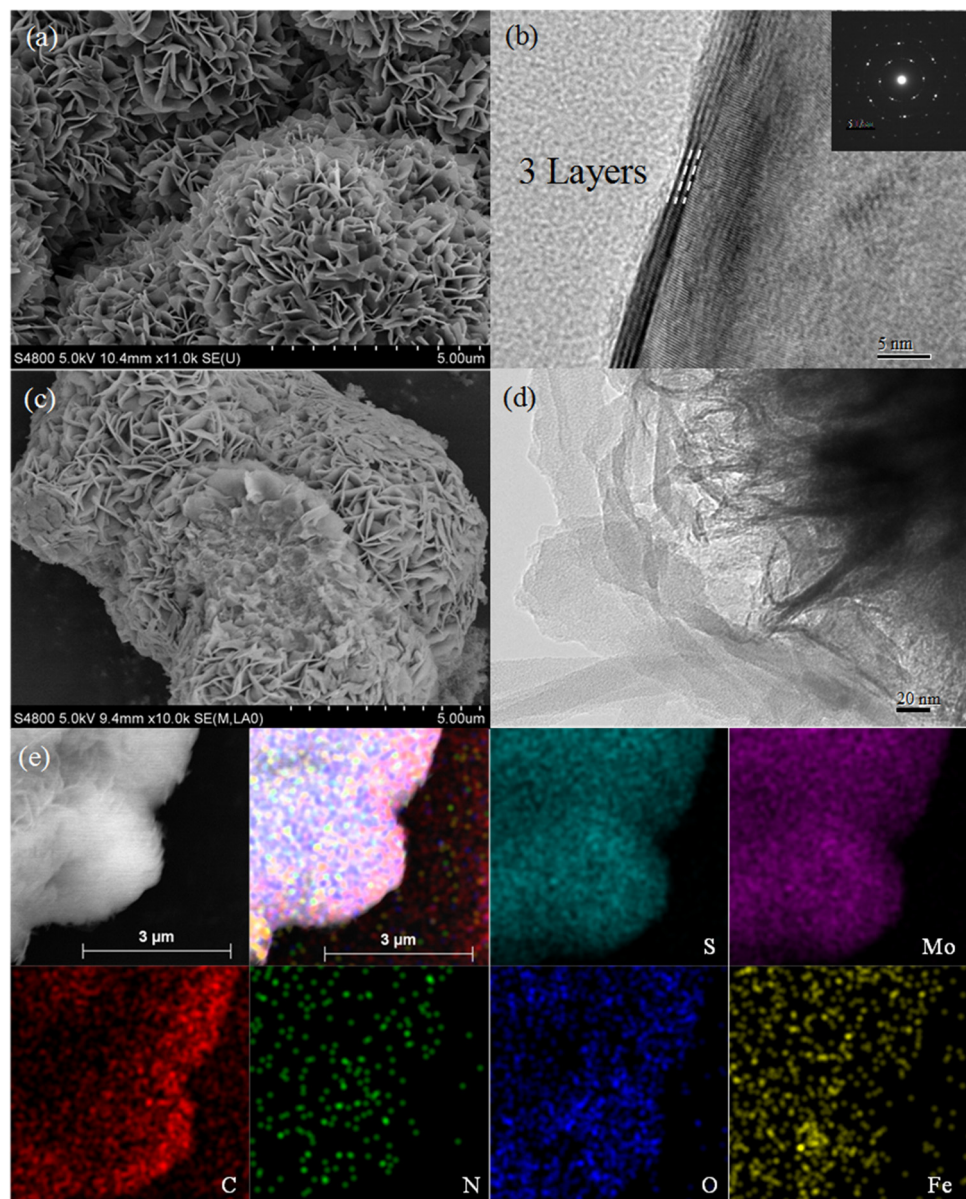


**Fig. 1.** SEM image of (a) MoS<sub>2</sub> and (c) 20% FeTCPP/MoS<sub>2</sub>. TEM image of (b) MoS<sub>2</sub> (The insert is SAED) and (d) 20% FeTCPP/MoS<sub>2</sub>. (e) EDX Mapping of 20% FeTCPP/MoS<sub>2</sub> sample.

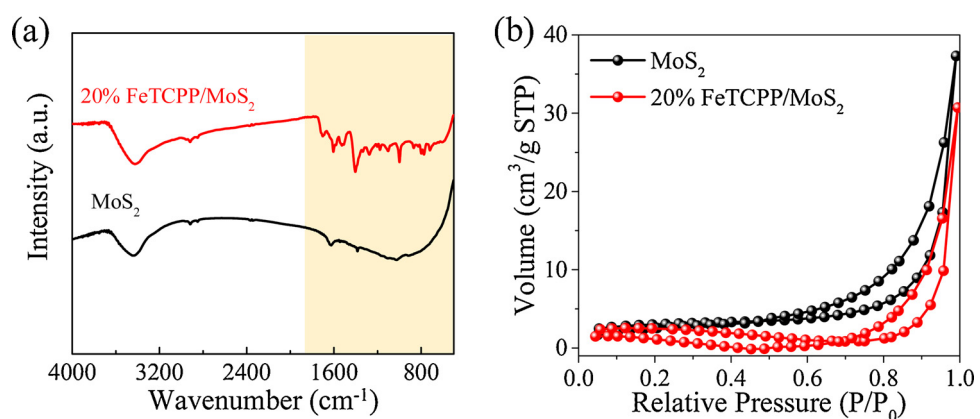


**Fig. 2.** (a) FTIR spectra of MoS<sub>2</sub> and 20% FeTCPP/MoS<sub>2</sub>. (b) N<sub>2</sub> adsorption-desorption isotherms of MoS<sub>2</sub> and 20% FeTCPP/MoS<sub>2</sub> samples.

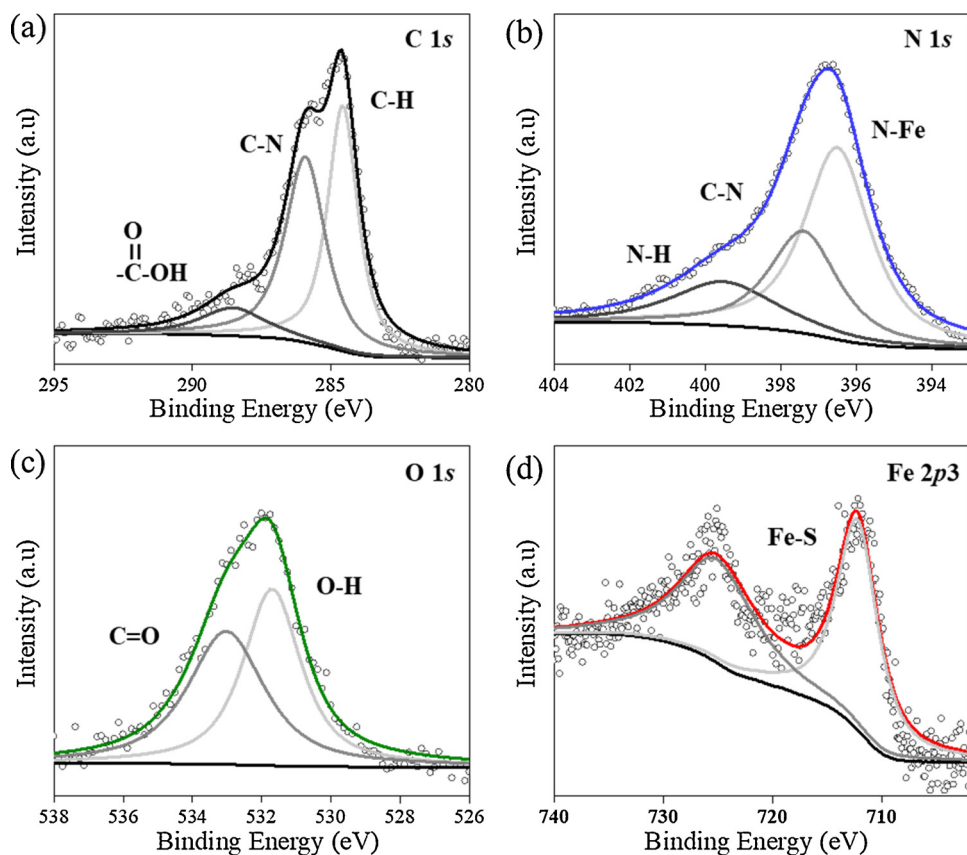


Fig. 3. XPS spectra of FeTCPP/MoS<sub>2</sub>. (a) C 1s, (b) N 1s, (c) O 1s and (d) Fe 2p3.

the specific surface area ( $S_{BET}$ ) of 20% FeTCPP/MoS<sub>2</sub> was decreased from 9.8 to 6.5 m<sup>2</sup> g<sup>-1</sup>, as well as  $V_p$  reduced from 0.057 to 0.046 cm<sup>3</sup> g<sup>-1</sup>. The peaks of C1s (C—H, C—N, COOH), N1s (N—C, N—H) and O1s (O—H, C=O) in the XPS survey spectra are the original on the porphyrin molecule (Fig. 3a–c). It should be noted here that the N-Fe peak appears because Fe becomes the porphyrin metal center (Fig. 3c) [60]. Interestingly, the formation of the Fe-S peak indicates a bond between the photosensitizer and the carrier, which may accelerate the electron transfer (Fig. 3d).

In order to further clarify the mode of charge carrier migration, transfer and separation, the photocurrent responses of bare MoS<sub>2</sub>,

TCPP/MoS<sub>2</sub> and FeTCPP/MoS<sub>2</sub> composite electrodes were tested. Fig. 4 reveals that the bare MoS<sub>2</sub> has almost no photocurrent, while FeTCPP/MoS<sub>2</sub> exhibits a higher photocurrent than TCPP/MoS<sub>2</sub> at steady state due to the effective photo-generated charge from Fe-S channel between FeTCPP and MoS<sub>2</sub>, which reduces the recombination of photogenerated carriers. This provides direct evidence of electron transfer from photoexcited FeTCPP to MoS<sub>2</sub>.

XRD analysis of FeTCPP/MoS<sub>2</sub> catalysts with different loadings was carried out. The results showed that MoS<sub>2</sub> surface modification of FeTCPP did not cause significant changes in XRD patterns, and the peak shape remains the characteristic absorption peaks of MoS<sub>2</sub> (PDF#77-1716).

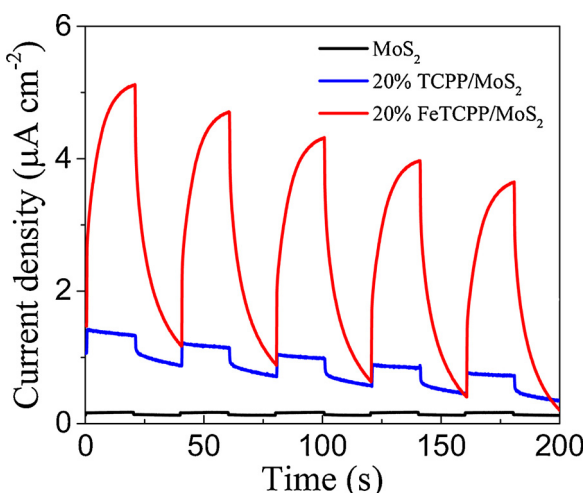


Fig. 4. Transient photocurrent responses of MoS<sub>2</sub>, TCPP/MoS<sub>2</sub> and FeTCPP/MoS<sub>2</sub> composite electrodes recorded in 0.5 M NaSO<sub>4</sub> aqueous solution under with light-on and light-off cycles.

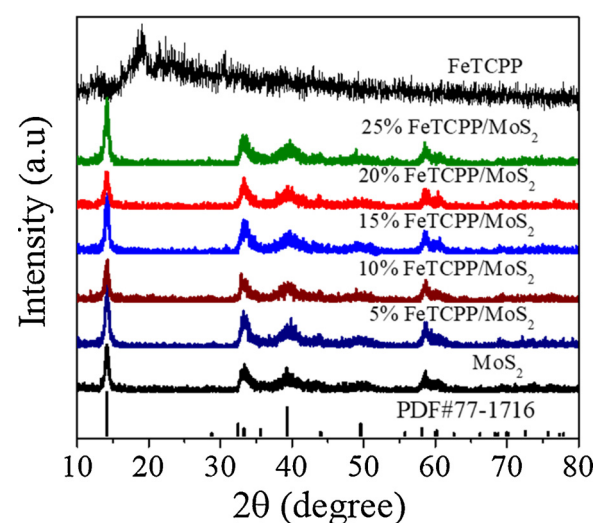


Fig. 5. XRD patterns of FeTCPP, MoS<sub>2</sub> and FeTCPP/MoS<sub>2</sub>.

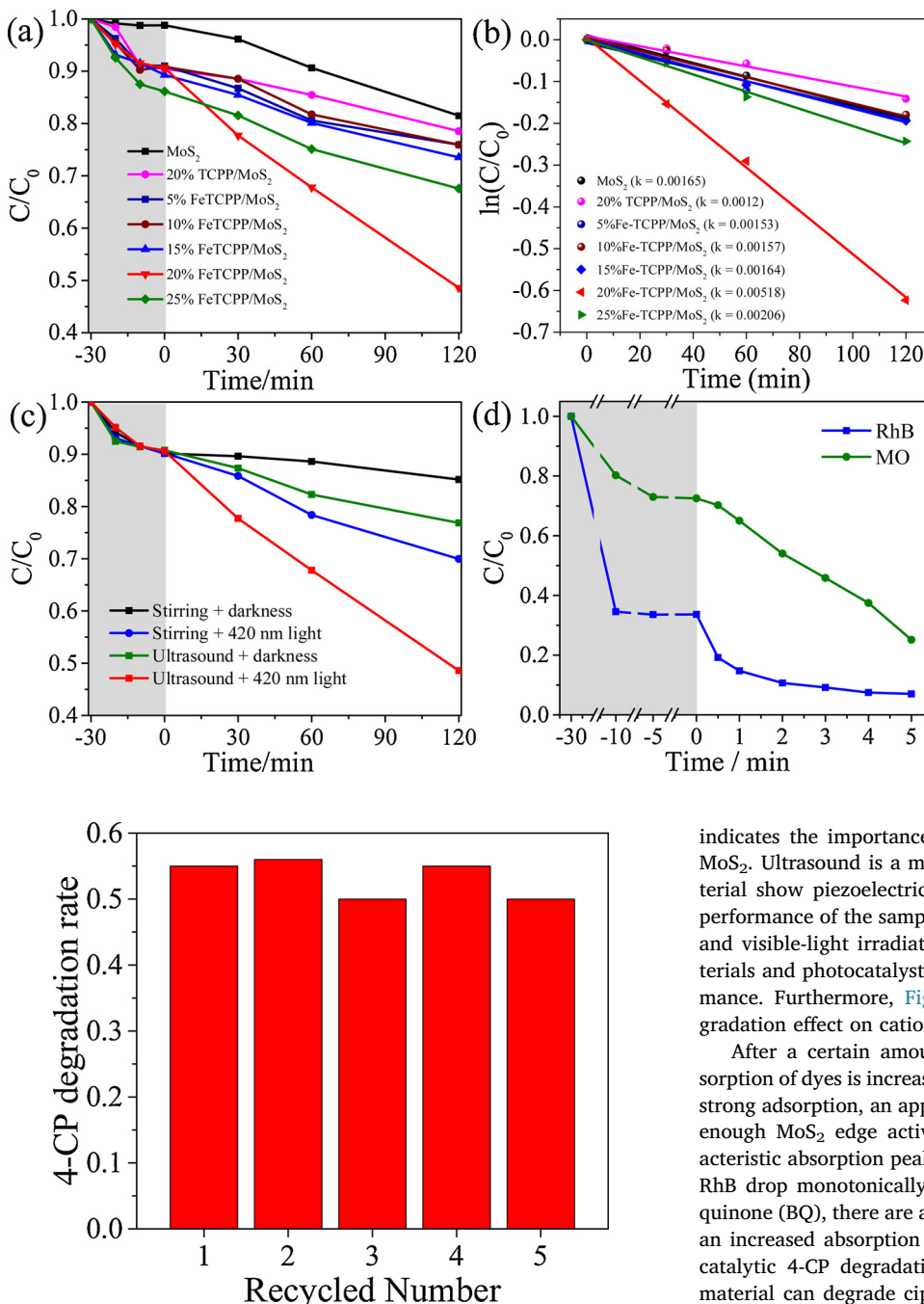


Fig. 7. The cycling degradation tests of the 4-CP (50 mL 10 ppm 4-CP, 50 mg 20% FeTCPP/MoS<sub>2</sub>, 1 atm air atmosphere, room temperature, ultrasonic-wave assistance with the 420 nm LED).

1716) (Fig. 5) [61].

To evaluate the visible light photocatalytic activity, 4-CP, RhB and MO were used as probes for simulating pollutants. (Fig. 6). Using 4-CP as an example, it is the representative of environmental refractory toxic organic pollutants. The results showed that the degradation activity of 20% FeTCPP/MoS<sub>2</sub> was 3.14 times higher than that of pure MoS<sub>2</sub> (Fig. 6a and b). With the increasing loading of FeTCPP (0%~20%), the photocatalytic activity increases continuously. However, the excessive loading (25%) will lead to the decrease of the photocatalytic activity. The main reason is that excessive porphyrin molecules will cover the active sites on the surface of MoS<sub>2</sub>, resulting in the reduction of photocatalytic activity. When the same content of TCPP replaces FeTCPP to modify MoS<sub>2</sub>, the photocatalytic activity decreases significantly, which

Fig. 6. Different photocatalytic degradation of 4-CP (a) and kinetic linear fitting curves of 4-CP (b) under the same reaction conditions (50 mL 10 ppm 4-CP, 50 mg catalyst, 1 atm air atmosphere, room temperature, ultrasonic-wave assistance with the 420 nm LED). (c) 20% FeTCPP/MoS<sub>2</sub> catalytic degradation of 4-CP under different reaction conditions. (d) 20% FeTCPP/MoS<sub>2</sub> catalytic degradation of RhB and MO under the same reaction conditions (50 mL 10 ppm RhB or MO, 50 mg catalyst, 1 atm air atmosphere, room temperature, ultrasonic-wave assistance with the 420 nm LED).

indicates the importance of electronic channel between FeTCPP and MoS<sub>2</sub>. Ultrasound is a means to make the surface of piezoelectric material show piezoelectric field. Fig. 6c shows that the photocatalytic performance of the samples is low without the assistance of ultrasound and visible-light irradiation. This indicates that the piezoelectric materials and photocatalysts can work together to maximize their performance. Furthermore, Fig. 6d displays that it also has a certain degradation effect on cationic dyes (RhB) and anionic dyes (MO).

After a certain amount (15%~25%) of FeTCPP is added, the adsorption of dyes is increased by more than 2 times. Under the premise of strong adsorption, an appropriate amount (20%) of FeTCPP can expose enough MoS<sub>2</sub> edge active sites (Fig. S3). From the spectra of characteristic absorption peaks, we observe that the absorption intensity of RhB drop monotonically (Fig. S4a). Due to the generation of benzoquinone (BQ), there are a decreased absorption intensity at 224 nm and an increased absorption intensity at 254 nm in the 2 h during photocatalytic 4-CP degradation (Fig. S4b) [62]. The 20% FeTCPP/MoS<sub>2</sub> material can degrade ciprofloxacin by 95% within 2 h (Figs. S4c and S4d). In the same concentration of ciprofloxacin (CPFX), the degradation rate of 20% FeTCPP/MoS<sub>2</sub> is significantly faster than that of KBrO<sub>3</sub> and CaBi<sub>6</sub>O<sub>10</sub>. For H<sub>4</sub>SiW<sub>12</sub>O<sub>40</sub>/TiO<sub>2</sub>/fly-ash (UV light photocatalysis), 20% FeTCPP/MoS<sub>2</sub> can achieve similar degradation rate with less catalyst under visible light irradiation. Furthermore, we summarize and contrast the existing combination of photocatalyst and piezoelectric catalysts for the degradation of contaminant rhodamine (RhB) and methyl orange (MO). The degradation efficiency of 20% FeTCPP/MoS<sub>2</sub> to RhB and MO is much higher than other piezoelectric-photocatalytic materials (Table S1).

Cycling test of sample is an important basis to show the catalytic stability of the sample. Fig. 7 shows that after five cyclic degradation tests, 20% FeTCPP/MoS<sub>2</sub> still maintains 50% 4-CP degradation rate with the assistance of ultrasound under visible light. The degradation rate of RhB and the removal rate of TOC can be maintained at 100% after five cycles (Fig. S5).

Currently, the commonly used mechanism of pollutant degradation

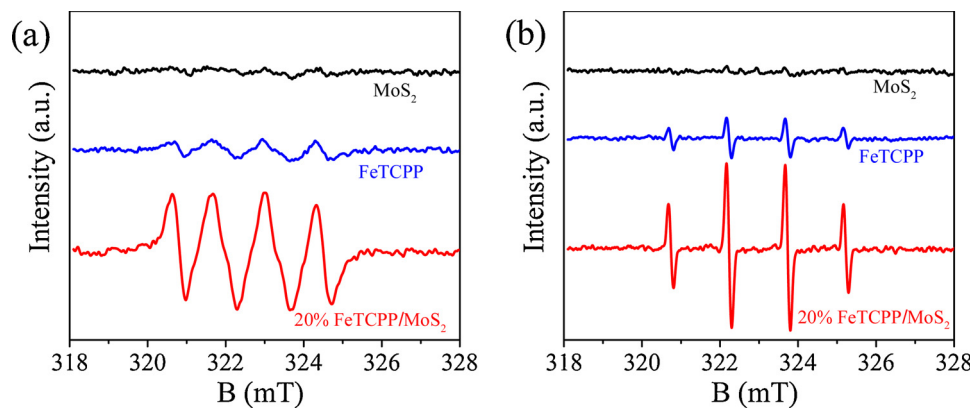


Fig. 8. ESR test for reactive oxygen species (ROS) under visible light (a)  $\cdot\text{O}_2^-$  species and (b)  $\cdot\text{OH}$  species.

is the oxidation of pollutant molecules by reactive oxygen species ( $\cdot\text{O}_2^-$  and  $\cdot\text{OH}$ ). Generally, electrons are trapped by oxygen to form superoxide radicals ( $\cdot\text{O}_2^-$ ), which react with water to form hydroxyl radicals ( $\cdot\text{OH}$ ) [63]. Electron spin resonance (ESR), a powerful analytical tool for exploring reactive oxygen species under various conditions, used to measure the type and amount of reactive oxygen species, thereby providing a direct indication of the increased degradation activity. As shown in Fig. 8, the FeTCPP/MoS<sub>2</sub> displayed the characteristic signals of  $\cdot\text{O}_2^-$  and  $\cdot\text{OH}$  have been greatly improved in contrast to MoS<sub>2</sub> and FeTCPP, supporting the observation of efficient co-catalytic activity of FeTCPP/MoS<sub>2</sub>.

The experimental results show that the piezoelectric properties of MoS<sub>2</sub> and the photocatalytic properties of FeTCPP can be effectively combined by the introduction of ultrasound under illumination, which is the main reason for the ultra-high degradation activity of pollutants. The schematic diagram clearly shows the electron transfer process (Fig. 9). Electrons on porphyrins are usually transferred from the side groups to the metal center. In the FeTCPP/MoS<sub>2</sub> system, the electrons are likely to be directly transferred from FeTCPP to the MoS<sub>2</sub> via the bond of Fe-S. Fig. S6 illustrates our proposed mechanism of the synergistic effect between MoS<sub>2</sub> and FeTCPP. First, the electrons generated by photoexcitation of FeTCPP tend to flow to MoS<sub>2</sub>, leaving the porphyrin molecules to protonize the contaminants. And then, the piezoelectric effect of MoS<sub>2</sub> under ultrasonic action can effectively separate electrons and holes so that hinder carrier recombination.

Respectively, electron and holes react with water and oxygen to form reactive oxygen species, thereby improving degradation activity [64].

#### 4. Conclusion

In summary, we have successfully prepared FeTCPP/MoS<sub>2</sub> catalysts with both photocatalytic activity and piezoelectric effect. By mechanical vibration (piezoelectric effect) and light irradiation (photocatalytic effect), the FeTCPP/MoS<sub>2</sub> catalyst can be triggered to generate more ROS ( $\cdot\text{OH}$  and  $\cdot\text{O}_2^-$ ). It uses the Fe-S connection between MoS<sub>2</sub> and FeTCPP to establish a new transmission path between the two substances. This special mode not only improves the efficiency of interface charge separation, but also enhances the light absorption capacity of the material. It is also possible to design a more effective multi-effect composite catalyst by this mode. The current understanding and outlook also open up new possibilities for manipulating the general aspects of the environment, energy, materials and catalytic science.

#### Declaration of Competing Interest

The authors declare that they have no known competing financial interests or personal relationships that could have appeared to influence the work reported in this paper.

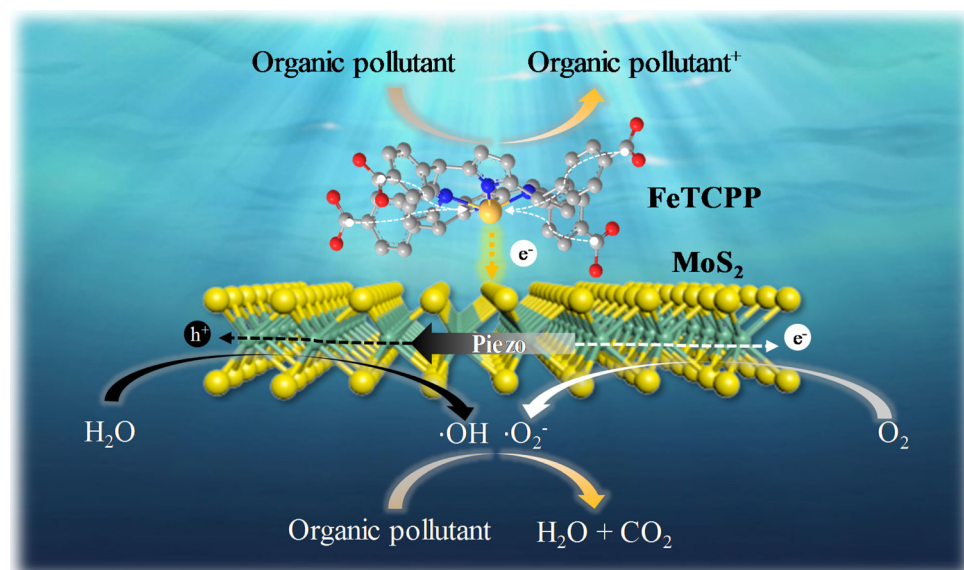


Fig. 9. Schematic of the FeTCPP/MoS<sub>2</sub> cocatalyst for degradation pollutant.

## Acknowledgments

This work was supported by the National Natural Science Foundation of China (21876114, 21761142011, 51572174), Shanghai Government (17SG44), International Joint Laboratory on Resource Chemistry (IJLRC), and Ministry of Education of China (PCSIRT\_IRT\_16R49). Research is also supported by The Program for Professor of Special Appointment (Eastern Scholar) at Shanghai Institutions of Higher Learning and Shuguang Research Program of Shanghai Education Committee.

## Appendix A. Supplementary data

Supplementary material related to this article can be found, in the online version, at doi:<https://doi.org/10.1016/j.apcatb.2019.118024>.

## References

- [1] M.A. Oturan, J.-J. Aaron, Advanced oxidation processes in water/wastewater treatment: principles and applications. A review, *Crit. Rev. Environ. Sci. Technol.* 44 (2014) 2577–2641.
- [2] D.B. Miklos, C. Remy, M. Jekel, K.G. Linden, J.E. Drewes, U. Hubner, Evaluation of advanced oxidation processes for water and wastewater treatment – a critical review, *Water Res.* 139 (2018) 118–131.
- [3] Z.M. Xu, R. Zheng, Y. Chen, J. Zhu, Z.F. Bian, Ordered mesoporous Fe/TiO<sub>2</sub> with light enhanced photo-Fenton activity, *Chin. J. Catal.* 40 (2019) 631–637.
- [4] Y.M. Dong, G.L. Wang, P.P. Jiang, A.M. Zhang, L. Yue, X.M. Zhang, Simple preparation and catalytic properties of ZnO for ozonation degradation of phenol in water, *Chin. Chem. Lett.* 22 (2011) 209–212.
- [5] X.L. Hao, L.Y. Zou, G.S. Zhang, Y.B. Zhang, Magnetic field assisted Fenton reactions for the enhanced degradation of methyl blue, *Chin. Chem. Lett.* 20 (2009) 99–101.
- [6] M. Xing, W. Xu, C. Dong, Y. Bai, J. Zeng, Y. Zhou, J. Zhang, Y. Yin, Metal sulfides as excellent co-catalysts for H<sub>2</sub>O<sub>2</sub> decomposition in advanced oxidation processes, *Chemistry* 4 (2018) 1–14.
- [7] S. Malato, P. Fernández-Ibáñez, M.I. Maldonado, J. Blanco, W. Gernjak, Decontamination and disinfection of water by solar photocatalysis: recent overview and trends, *Catal. Today* 147 (2009) 1–59.
- [8] D. Ravelli, D. Dondi, M. Fagnoni, A. Albini, Photocatalysis. A multi-faceted concept for green chemistry, *Chem. Soc. Rev.* 38 (2009) 1999–2011.
- [9] T. Yang, J. Peng, Y. Zheng, X. He, Y. Hou, L. Wu, X. Fu, Enhanced photocatalytic ozonation degradation of organic pollutants by ZnO modified TiO<sub>2</sub> nanocomposites, *Appl. Catal. B-Environ.* 221 (2018) 223–234.
- [10] R. Dewil, D. Mantzavinos, I. Poulios, M.A. Rodrigo, New perspectives for advanced oxidation processes, *J. Environ. Manage.* 195 (2017) 93–99.
- [11] S.G. Kumar, L.G. Devi, Review on modified TiO<sub>2</sub> photocatalysis under UV/visible light: selected results and related mechanisms on interfacial charge carrier transfer dynamics, *J. Phys. Chem. A* 115 (2011) 13211–13241.
- [12] R. Marschall, Semiconductor composites: strategies for enhancing charge carrier separation to improve photocatalytic activity, *Adv. Funct. Mater.* 24 (2014) 2421–2440.
- [13] G. Yin, X. Huang, T. Chen, W. Zhao, Q. Bi, J. Xu, Y. Han, F. Huang, Hydrogenated blue titania for efficient solar to chemical conversions: preparation, characterization, and reaction mechanism of CO<sub>2</sub> reduction, *ACS Catal.* (2018) 1009–1017.
- [14] Y. Yang, L.-C. Yin, Y. Gong, P. Niu, J.-Q. Wang, L. Gu, X. Chen, G. Liu, L. Wang, H.-M. Cheng, An unusual strong visible-light absorption band in red anatase TiO<sub>2</sub> photocatalyst induced by atomic hydrogen-occupied oxygen vacancies, *Adv. Mater.* (2018) 1704479.
- [15] J. Wan, W. Chen, C. Jia, L. Zheng, J. Dong, X. Zheng, Y. Wang, W. Yan, C. Chen, Q. Peng, D. Wang, Y. Li, Defect effects on TiO<sub>2</sub> nanosheets: stabilizing single atomic site au and promoting catalytic properties, *Adv. Mater.* (2018) 1705369.
- [16] H. Yu, R. Shi, Y. Zhao, T. Bian, Y. Zhao, C. Zhou, G.I.N. Waterhouse, L.Z. Wu, C.H. Tung, T. Zhang, Alkali-assisted synthesis of nitrogen deficient graphitic carbon nitride with tunable band structures for efficient visible-light-driven hydrogen evolution, *Adv. Mater.* 29 (2017) 1605148.
- [17] H. Li, J. Shang, Z. Ai, L. Zhang, Efficient visible light nitrogen fixation with BiOBr nanosheets of oxygen vacancies on the exposed {001} facets, *J. Am. Chem. Soc.* 137 (2015) 6393–6399.
- [18] S. Wang, L. Pan, J.J. Song, W. Mi, J.J. Zou, L. Wang, X. Zhang, Titanium-defected undoped anatase TiO<sub>2</sub> with p-type conductivity, room-temperature ferromagnetism, and remarkable photocatalytic performance, *J. Am. Chem. Soc.* 137 (2015) 2975–2983.
- [19] H. Li, F. Qin, Z. Yang, X. Cui, J. Wang, L. Zhang, New reaction pathway induced by plasmon for selective benzyl alcohol oxidation on BiOCl possessing oxygen vacancies, *J. Am. Chem. Soc.* 139 (2017) 3513–3521.
- [20] D.-I. Won, J.-S. Lee, Q. Ba, Y.-J. Cho, H.-Y. Cheong, S. Choi, C.H. Kim, H.-J. Son, C. Pac, S.O. Kang, Development of a lower energy photosensitizer for photocatalytic CO<sub>2</sub> reduction: modification of porphyrin dye in hybrid catalyst system, *ACS Catal.* (2018) 1018–1030.
- [21] P.Y. Ho, M.F. Mark, Y. Wang, S.C. Yiu, W.H. Yu, C.L. Ho, D.W. McCamant, R. Eisenberg, S. Huang, Panchromatic sensitization with Zn(II) porphyrin-based photosensitizers for light-driven hydrogen production, *ChemSusChem* 11 (2018) 2517–2528.
- [22] F. Theil, A. Dellith, J. Dellith, A. Undisz, A. Csaki, W. Fritzsche, J. Popp, M. Rettenmayr, B. Dietzek, Ru dye functionalized Au-SiO<sub>2</sub>@TiO<sub>2</sub> and Au/Pt-SiO<sub>2</sub>@TiO<sub>2</sub> nanoassemblies for surface-plasmon-induced visible light photocatalysis, *J. Colloid Interface Sci.* 421 (2014) 114–121.
- [23] Y.Z. Chen, Z.U. Wang, H. Wang, J. Lu, S.H. Yu, H.L. Jiang, Singlet oxygen-engaged selective photo-oxidation over Pt nanocrystals/porphyrinic MOF: the roles of photothermal effect and Pt electronic state, *J. Am. Chem. Soc.* 139 (2017) 2035–2044.
- [24] Z. Zheng, T. Tachikawa, T. Majima, Plasmon-enhanced formic acid dehydrogenation using anisotropic Pd-Au nanorods studied at the single-particle level, *J. Am. Chem. Soc.* 137 (2015) 948–957.
- [25] B. Wu, D. Liu, S. Mubeen, T.T. Chuong, M. Moskovits, G.D. Stucky, Anisotropic growth of TiO<sub>2</sub> onto gold nanorods for plasmon-enhanced hydrogen production from water reduction, *J. Am. Chem. Soc.* 138 (2016) 1114–1117.
- [26] D. Kalyani, K.B. McMurtrey, S.R. Neufeldt, M.S. Sanford, Room-temperature C-H arylation: merger of Pd-catalyzed C-H functionalization and visible-light photocatalysis, *J. Am. Chem. Soc.* 133 (2011) 18566–18569.
- [27] X. Liu, J. Icoozzia, Y. Wang, X. Cui, Y. Chen, S. Zhao, Z. Li, Z. Lin, Noble metal–metal oxide nanohybrids with tailored nanostructures for efficient solar energy conversion, photocatalysis and environmental remediation, *Energy Environ. Sci.* 10 (2017) 402–434.
- [28] Y. Zhang, M. Xu, H. Li, H. Ge, Z. Bian, The enhanced photoreduction of Cr(VI) to Cr(III) using carbon dots coupled TiO<sub>2</sub> mesocrystals, *Appl. Catal. B-Environ.* 226 (2018) 213–219.
- [29] K. Woan, G. Pyrgiotakis, W. Sigmund, Photocatalytic carbon-nanotube-TiO<sub>2</sub> composites, *Adv. Mater.* 21 (2009) 2233–2239.
- [30] J. Liu, Y. Liu, N. Liu, Y. Han, X. Zhang, H. Huang, Y. Lifshitz, S.-T. Lee, J. Zhong, Z. Kang, Metal-free efficient photocatalyst for stable visible water splitting via a two-electron pathway, *Science* 347 (2015) 970–974.
- [31] H. Wang, L. Zhang, Z. Chen, J. Hu, S. Li, Z. Wang, J. Liu, X. Wang, Semiconductor heterojunction photocatalysts: design, construction, and photocatalytic performances, *Chem. Soc. Rev.* 43 (2014) 5234–5244.
- [32] Q. Wang, T. Hisatomi, Q. Jia, H. Tokudome, M. Zhong, C. Wang, Z. Pan, T. Takata, M. Nakabayashi, N. Shibata, Y. Li, I.D. Sharp, A. Kudo, T. Yamada, K. Domen, Scalable water splitting on particulate photocatalyst sheets with a solar-to-hydrogen energy conversion efficiency exceeding, *Nat. Mater.* 15 (2016) 611–615.
- [33] H. He, J. Lin, W. Fu, X. Wang, H. Wang, Q. Zeng, Q. Gu, Y. Li, C. Yan, B.K. Tay, C. Xue, X. Hu, S.T. Pantelides, W. Zhou, Z. Liu, MoS<sub>2</sub>/TiO<sub>2</sub> edge-nn heterostructure for efficient photocatalytic hydrogen evolution, *Adv. Energy Mater.* 6 (2016) 1600464.
- [34] S. Xie, Z. Shen, J. Deng, P. Guo, Q. Zhang, H. Zhang, C. Ma, Z. Jiang, J. Cheng, D. Deng, Y. Wang, Visible light-driven C-H activation and C-C coupling of methanol into ethylene glycol, *Nat. Commun.* 9 (2018) 1181–1188.
- [35] C. Chen, W. Cai, M. Long, B. Zhou, Y. Wu, D. Wu, Y. Feng, Synthesis of visible-light responsive graphene oxide-TiO<sub>2</sub> composites with p-n heterojunction, *ACS Nano* 4 (2010) 6425–6432.
- [36] J. Chen, C.L. Dong, D. Zhao, Y.C. Huang, X. Wang, L. Samad, L. Dang, M. Shearer, S. Shen, L. Guo, Molecular design of polymer heterojunctions for efficient solar-hydrogen conversion, *Adv. Mater.* 29 (2017) 1606198.
- [37] Y.-Y. Han, X.-L. Lu, S.-F. Tang, X.-P. Yin, Z.-W. Wei, T.-B. Lu, Metal-free 2D/2D heterojunction of graphitic carbon nitride/graphdiyne for improving the hole mobility of graphitic carbon nitride, *Adv. Energy Mater.* (2018) 1702992.
- [38] L. Ge, C. Han, J. Liu, Novel visible light-induced g-C<sub>3</sub>N<sub>4</sub>/Bi<sub>2</sub>WO<sub>6</sub> composite photocatalysts for efficient degradation of methyl orange, *Appl. Catal. B-Environ.* 108–109 (2011) 100–107.
- [39] J. Low, J. Yu, M. Jaroniec, S. Wageh, A.A. Al-Ghamdi, Heterojunction photocatalysts, *Adv. Mater.* 29 (2017) 1601694.
- [40] S. Hiroto, Y. Miyake, H. Shinokubo, Synthesis and functionalization of porphyrins through organometallic methodologies, *Chem. Rev.* 117 (2017) 2910–3043.
- [41] T. Tanaka, A. Osuka, Conjugated porphyrin arrays: synthesis, properties and applications for functional materials, *Chem. Soc. Rev.* 44 (2015) 943–969.
- [42] S. Saito, A. Osuka, Expanded porphyrins: intriguing structures, electronic properties, and reactivities, *Angew. Chem. Int. Ed. English* 50 (2011) 4342–4373.
- [43] O.P. Charkin, N.M. Klimenko, D.O. Charkin, Y.S. Wang, S.C. Wei, H.C. Chang, S.H. Lin, Theoretical study of the structure and stability of the ferrisporphyrin dimer [Fe(III)C<sub>34</sub>H<sub>31</sub>N<sub>4</sub>O<sub>4</sub>]<sub>2</sub>, *Russ. J. Inorg. Chem.* 51 (2006) 89–98.
- [44] Y. Huang, F. Zhuge, J. Hou, L. Lv, P. Luo, N. Zhou, L. Gan, T. Zhai, Van der waals coupled organic molecules with monolayer MoS<sub>2</sub> for fast response photodetectors with gate-tunable responsivity, *ACS Nano* 12 (2018) 4062–4073.
- [45] Y. Fang, X. Hu, W. Zhao, J. Pan, D. Wang, K. Bu, Y. Mao, S. Chu, P. Liu, T. Zhai, F. Huang, Structural determination and nonlinear optical properties of new 1T"-type MoS<sub>2</sub> compound, *J. Am. Chem. Soc.* 141 (2019) 790–793.
- [46] J. Shi, R. Tong, X. Zhou, Y. Gong, Z. Zhang, Q. Ji, Y. Zhang, Q. Fang, L. Gu, X. Wang, Z. Liu, Y. Zhang, Temperature-mediated selective growth of MoS<sub>2</sub>/WS<sub>2</sub> and WS<sub>2</sub>/MoS<sub>2</sub> vertical stacks on Au foils for direct photocatalytic applications, *Adv. Mater.* 28 (2016) 10664–10672.
- [47] W. Wu, L. Wang, Y. Li, F. Zhang, L. Lin, S. Niu, D. Chenet, X. Zhang, Y. Hao, T.F. Heinz, J. Hone, Z.L. Wang, Piezoelectricity of single-atomic-layer MoS<sub>2</sub> for energy conversion and piezotronics, *Nature* 514 (2014) 470–474.
- [48] L. Guo, Z. Yang, K. Marcus, Z. Li, B. Luo, L. Zhou, X. Wang, Y. Du, Y. Yang, MoS<sub>2</sub>/TiO<sub>2</sub> heterostructures as nonmetal plasmonic photocatalysts for highly efficient hydrogen evolution, *Energy Environ. Sci.* 11 (2018) 106–114.
- [49] J. Li, G. Zhan, Y. Yu, L. Zhang, Superior visible light hydrogen evolution of Janus bilayer junctions via atomic-level charge flow steering, *Nat. Commun.* 7 (2016) 11480.

[50] J.M. Wu, W.E. Chang, Y.T. Chang, C.K. Chang, Piezo-catalytic effect on the enhancement of the ultra-high degradation activity in the dark by single- and few-layers MoS<sub>2</sub> nanoflowers, *Adv. Mater.* 28 (2016) 3718–3725.

[51] Y. Feng, L. Ling, J. Nie, K. Han, X. Chen, Z. Bian, H. Li, Z.L. Wang, Self-powered electrostatic filter with enhanced photocatalytic degradation of formaldehyde based on built-in triboelectric nanogenerators, *ACS Nano* 11 (2017) 12411–12418.

[52] Y. Feng, H. Li, L. Ling, S. Yan, D. Pan, H. Ge, H. Li, Z. Bian, Enhanced photocatalytic degradation performance by fluid-induced piezoelectric field, *Environ. Sci. Technol.* 52 (2018) 7842–7848.

[53] S. Jia, Y. Su, B. Zhang, Z. Zhao, S. Li, Y. Zhang, P. Li, M. Xu, R. Ren, Few-layer MoS<sub>2</sub> nanosheet-coated KNbO<sub>3</sub> nanowire heterostructures: piezo-photocatalytic effect enhanced hydrogen production and organic pollutant degradation, *Nanoscale* 11 (2019) 7690–7700.

[54] T.-M. Chou, S.-W. Chan, Y.-J. Lin, P.-K. Yang, C.-C. Liu, Y.-J. Lin, J.-M. Wu, J.-T. Lee, Z.-H. Lin, A highly efficient Au-MoS<sub>2</sub> nanocatalyst for tunable piezocatalytic and photocatalytic water disinfection, *Nano Energy* 57 (2019) 14–21.

[55] Y. Zhang, C. Liu, G. Zhu, X. Huang, W. Liu, W. Hu, M. Song, W. He, J. Liu, J. Zhai, Piezotronic-effect-enhanced Ag<sub>2</sub>S/ZnO photocatalyst for organic dye degradation, *RSC Adv.* 7 (2017) 48176–48183.

[56] H. Li, Y. Sang, S. Chang, X. Huang, Y. Zhang, R. Yang, H. Jiang, H. Liu, Z.L. Wang, Enhanced ferroelectric-nanocrystal-based hybrid photocatalysis by ultrasonic-wave-generated piezophototronic effect, *Nano Lett.* 15 (2015) 2372–2379.

[57] L. Wang, S. Liu, Z. Wang, Y. Zhou, Y. Qin, Z.L. Wang, Piezotronic effect enhanced photocatalysis in strained anisotropic ZnO/TiO<sub>2</sub> nanoplatelets via thermal stress, *ACS Nano* 10 (2016) 2636–2643.

[58] C.F. Tan, W.L. Ong, G.W. Ho, Self-biased hybrid piezoelectric-photoelectrochemical cell with photocatalytic functionalities, *ACS Nano* 9 (2015) 7661–7670.

[59] A. Ikezaki, M. Takahashi, M. Nakamura, Equilibrium between Fe(IV) porphyrin and Fe(III) porphyrin radical cation: new insight into the electronic structure of high-valent iron porphyrin complexes, *Chem. Commun. (Camb.)* 49 (2013) 3098–3100.

[60] L. Lin, C. Hou, X. Zhang, Y. Wang, Y. Chen, T. He, Highly efficient visible-light driven photocatalytic reduction of CO<sub>2</sub> over g-C<sub>3</sub>N<sub>4</sub> nanosheets/tetra(4-carboxyphenyl)porphyrin iron(III) chloride heterogeneous catalysts, *Appl. Catal. B-Environ.* 221 (2018) 312–319.

[61] K. Chang, X. Hai, H. Pang, H. Zhang, L. Shi, G. Liu, H. Liu, G. Zhao, M. Li, J. Ye, Targeted synthesis of 2H- and 1T-phase MoS<sub>2</sub> monolayers for catalytic hydrogen evolution, *Adv. Mater.* 28 (2016) 10033–10041.

[62] M. Xu, Y. Chen, J. Qin, Y. Feng, W. Li, W. Chen, J. Zhu, H. Li, Z. Bian, Unveiling the role of defects on oxygen activation and photodegradation of organic pollutants, *Environ. Sci. Technol.* 52 (2018) 13879–13886.

[63] Y. Nosaka, A.Y. Nosaka, Generation and detection of reactive oxygen species in photocatalysis, *Chem. Rev.* 117 (2017) 11302–11336.

[64] G. Lan, Y.Y. Zhu, S.S. Veroneau, Z. Xu, D. Micheroni, W. Lin, Electron injection from photoexcited metal-organic framework ligands to Ru<sub>2</sub> secondary building units for visible-light-driven hydrogen evolution, *J. Am. Chem. Soc.* 140 (2018) 5326–5329.